Supplementary Information For:

Wildfire activity enhanced during phases of maximum orbital eccentricity and precessional forcing in the Early Jurassic

Teuntje P. Hollaar[a,b,*], Sarah J. Baker[a], Stephen P. Hesselbo[b,c], Jean-François Deconinck[d], Luke Mander[e], Micha Ruhl[f], and Claire M. Belcher[a]

[a]*WildFIRE Lab, Global Systems Institute, University of Exeter, Exeter, UK,* e-mail: t.p.hollaar@exeter.ac.uk

[b]*Camborne School of Mines, University of Exeter, Penryn Campus, UK*

[c]*Environment and Sustainability Institute, University of Exeter, Penryn Campus, UK*

[d] *Biogéosciences, Université de Bourgogne/Franche-Comté, Dijon, France*

[e]*Department of Environment, Earth and Ecosystems, The Open University, Milton Keynes, UK*

[f]*Department of Geology, Trinity College Dublin, The University of Dublin, Dublin, Ireland*

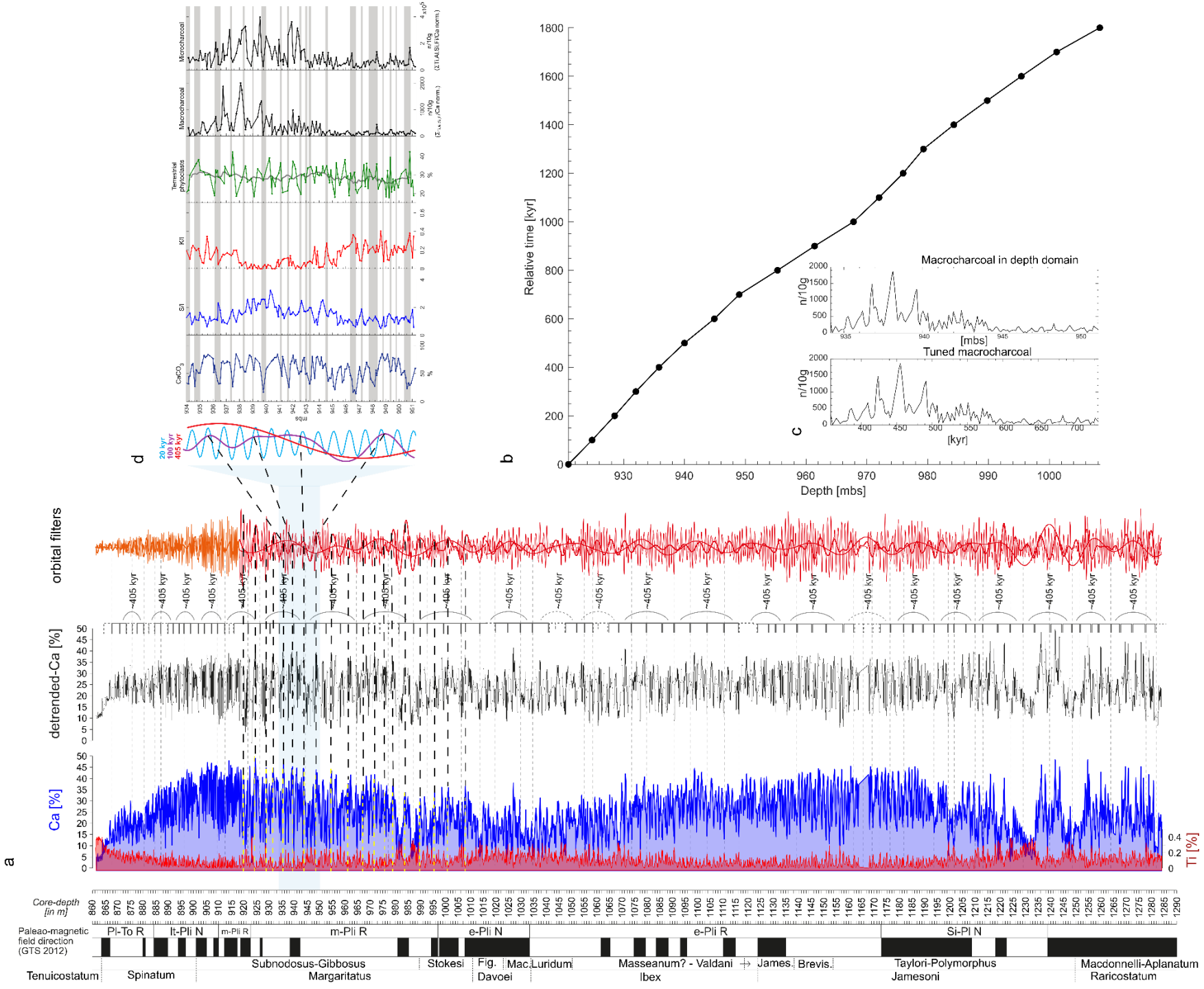
a
b
c
d
Macrocharcoal
Terrestrial phytoclasts
KI
SI
CaCO3
Relative time [kyr]
Depth [mbs]
Macrocharcoal in depth domain
Tuned macrocharcoal
[mbs]
[kyr]
20 kyr
100 kyr
405 kyr
orbital filters
~405 kyr
detrended-Ca [%]
Ca [%]
Ti [%]
Core-depth [in m]
Paleao-magnetic field direction (GTS 2012)
Pl-To R
It-Pli N
m-Pli R
e-Pli N
e-Pli R
Si-Pl N
Tenuicostatum
Spinatum
Subnodosus-Gibbosus
Margaritatus
Stokesi
Fig.
Davoei
Mac.
Luridum
Masseanum? - Valdani
Ibex
James.
Brevis.
Taylori-Polymorphus
Jamesoni
Macdonnelli-Aplanatum
Raricostatum

Supplementary Fig. 1: The studied interval placed in the existing cyclostratigraphic framework from Ruhl *et al*.[1]. (A) The cyclostratigraphic study of Ruhl *et al*.[1] based on XRF elemental concentrations (Ca, Ti) shows the presence of clear lithological bundling, which have been interpreted as the expression of the precession (20 kyr), short eccentricity (100 kyr) and long eccentricity (400 kyr). According to this interpretation, the depth domain was converted to a floating time series based on the peak ratios of 1:4:5 and tie points were created at the peaks of the stable 405 kyr cycle[1]. The record was tuned to the proposed astronomical solutions for this period (e.g. [2]), using radiometric tie points from the Peru and Hartford and Newark Basins (references within [1]). The record presented in this study fits in almost one complete long eccentricity cycle (~350 kyr; linked to long eccentricity cycle 459 ± 1 Fig. S2, cf. [3,4,5]).
The studied interval, which spans a ~17 m interval within the Margaritatus zone of the Pliensbachian stage, the elemental XRF Ca-record of Ruhl *et al*.[1] was further tuned to the peaks of the 100 kyr eccentricity cycle. This created 19 tie points, between ~1310 mbs at the start of the Margaritatus zone to ~920 mbs, which reaches into the Spinatum zone, where a change in sedimentation rate occurs. The stratigraphic context of these tie points are indicated in the figure by the dashed yellow/black lines.
(B) The age model plotted in Acycle[6], using the 'Show Age' model plot function within the 'Age Scale' function. This shows the relative time (kyr) versus depth (mbs) over the selected interval (~920–1008 mbs), with the selected tie points marked on the line graph. (C) The age model was used to convert the macrocharcoal (and the Ca, illite, percentage terrestrial phytoclasts and microcharcoal record) to the time domain. This graph shows the macrocharcoal record in depth domain (right) and time domain (left). (D) The shaded area, indicated in the larger framework of the cyclostratigraphic study by Ruhl *et al*.[1], spans the interval studied here. The orbital filters (20 kyr, 100 kyr and 400 kyr) are derived from Ruhl *et al*.[1] and have been plotted next to the synthetic diagram of the here studied interval (934-951 mbs) in cyclostratigraphic context. Four tie points (out of the 19 tie points for the Margaritatus zone) overlap with the presented study interval and are indicated by the black dashed lines.
The cyclostratigraphic analysis of Ruhl *et al*.,[1] has been further confirmed by an independent study of the $\delta^{13}C_{org}$ record in Mochras , showing the presence of 100 kyr and 405 kyr cycles[7] and a range of power spectral analyses of the Ca time series data, including a discussion of the red noise models used[8].

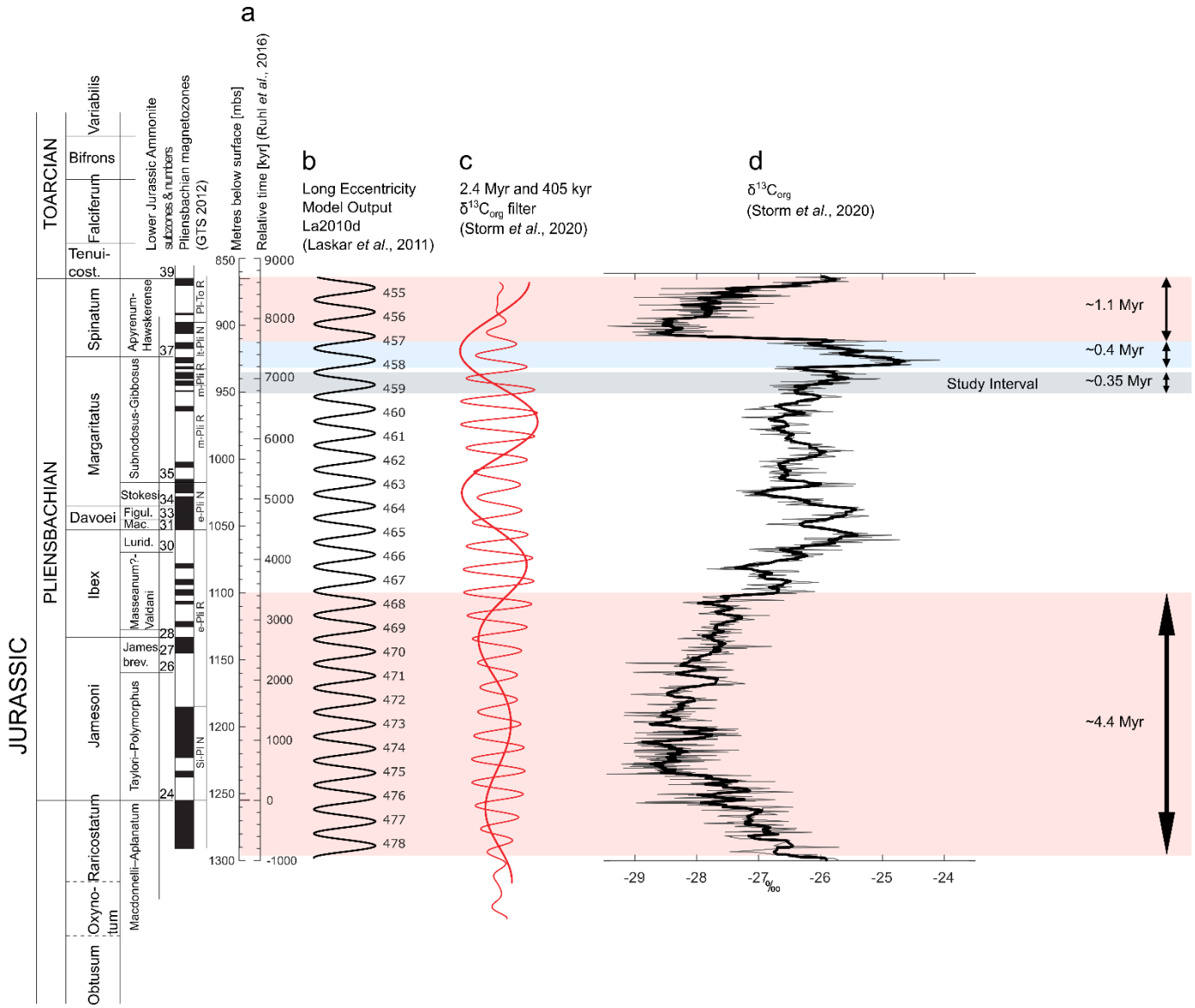

Supplementary Fig. 2: Cyclostratigraphic context of the studied interval. (A) Relative time (kyr), based on the tuned 405 kyr eccentricity cycle of the Ca record of Ruhl *et al.*[1], next to depth (mbs) of the Mochras borehole. (B) Long eccentricity model output derived from the orbital solution La2010d[2], showing that the studied interval comprises the long eccentricity cycle 459 ± 1. (C) The filtered 2.4 Myr and 405 kyr cycle from the bulk organic carbon isotope record from the Mochras borehole[7]. (D) The bulk organic carbon isotope record from Storm *et al.*[7] encompassing the entire Early Jurassic of the Mochras borehole. The here studied interval is marked with a grey shaded area and does not contain a major shift in the bulk organic carbon isotope record. Based on the La2010d astronomical solution[2] and the bulk organic carbon isotope excursion[7]: the Sinemurian-Pliensbachian boundary event lasts ~4.4 Myr, the Late Pliensbachian event spans one long eccentricity cycle (0.4 Myr) and the Spinatum event lasts ~1.1 Myr.

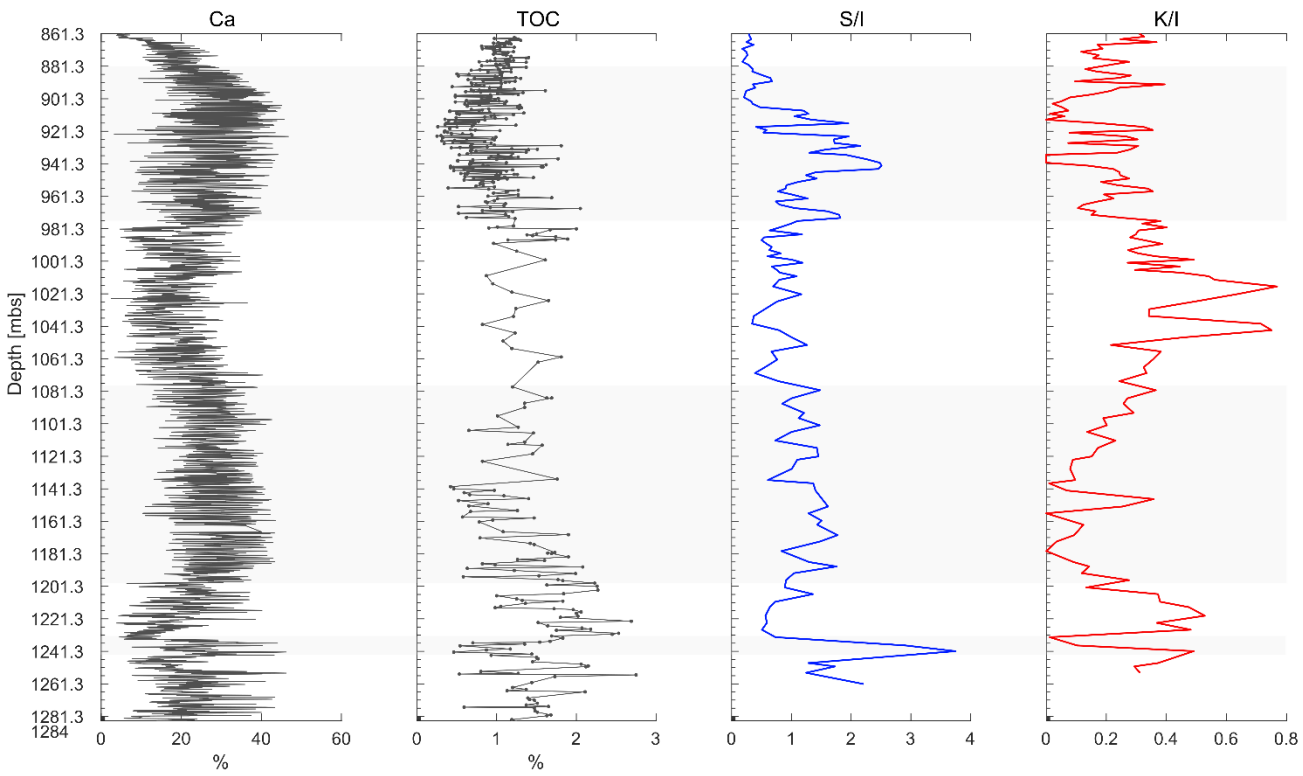

Supplementary Fig. 3: Variations in the proportions of Ca[1] and TOC[7], in comparison with variations in the smectite/illite (S/I) and kaolinite/illite (K/I) ratios[8] during the Pliensbachian of the Mochras borehole. The Ca and TOC abundance show an inverse trend during the Pliensbachian stage in the Mochras borehole. Intervals enriched in Ca are shaded in light grey and correspond to lower TOC values. The unshaded depths mark intervals that are relatively low in Ca and TOC-enriched. Moreover, the Ca-rich intervals from the Pliensbachian stage show a clear correspondence with smectite abundance[8]. Ca-rich intervals are observed between ~882–976 mbs, ~1076–1198 mbs and ~1232–1245 mbs and are coeval with high values of S/I (smectite/illite ratio). Furthermore, the intervals that contain relatively low Ca (TOC-enriched) show peak values in K/I (kaolinite/illite ratio). Deconinck *et al*.[8] interpret these long term changes in clay mineralogy to reflect changes in the hydrological cycle, with alternations of kaolinite-rich wet periods (acceleration of the hydrological cycle), and semi-arid periods rich in smectite, in which the runoff and terrigenous inputs were smaller and carbonate sedimentation was better expressed. The correspondence of Ca and smectite is also found in the high resolution, but relative short duration, of the here studied interval on the ~405 kyr time scale (Fig. 2 and Fig. S7).

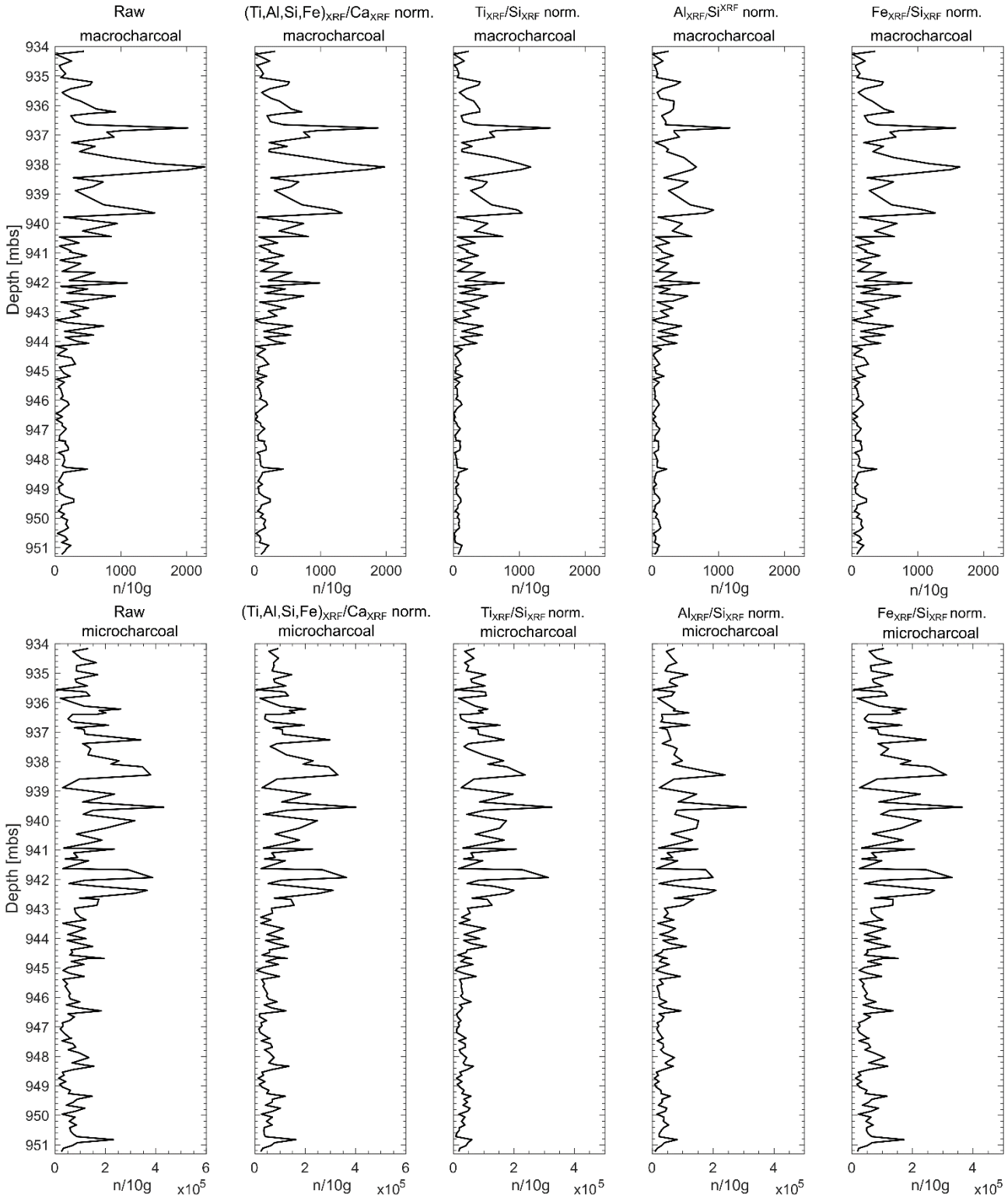

Supplementary Fig. 4: The same charcoal abundance pattern has been observed for the raw charcoal dataset, in comparison with the charcoal abundance records that were normalized to terrestrial influx and carbonate dilution (both on short and long scale). Long (mid-interval) and short (~1 m) cyclic variations are observed in the raw charcoal count

(particle number/10 g of processed sediment). The charcoal abundance record that has been normalized to terrigenous elements (Ti, Al, Si and Fe) and Ca shows the same cyclic patterns as the raw charcoal abundance record. This indicates that the cycles observed in the raw charcoal data are not affected by the terrigenous/biogenic ratio. Moreover, the normalization of the charcoal to terrigenous only ratios (Ti/Si, Al/Si and Fe/Si), shows the pattern of the long and short cycles is the same as the raw charcoal abundance and the $(Si+Ti+Al+Fe)_{XRF}$ / Ca_{XRF} normalized charcoal record. Therefore, for both the macro- and micro-charcoal fractions, the observed cyclicity is an indication of the production of the charcoal and not a preservational effect of the terrigenous/biogenic sedimentation cycle.

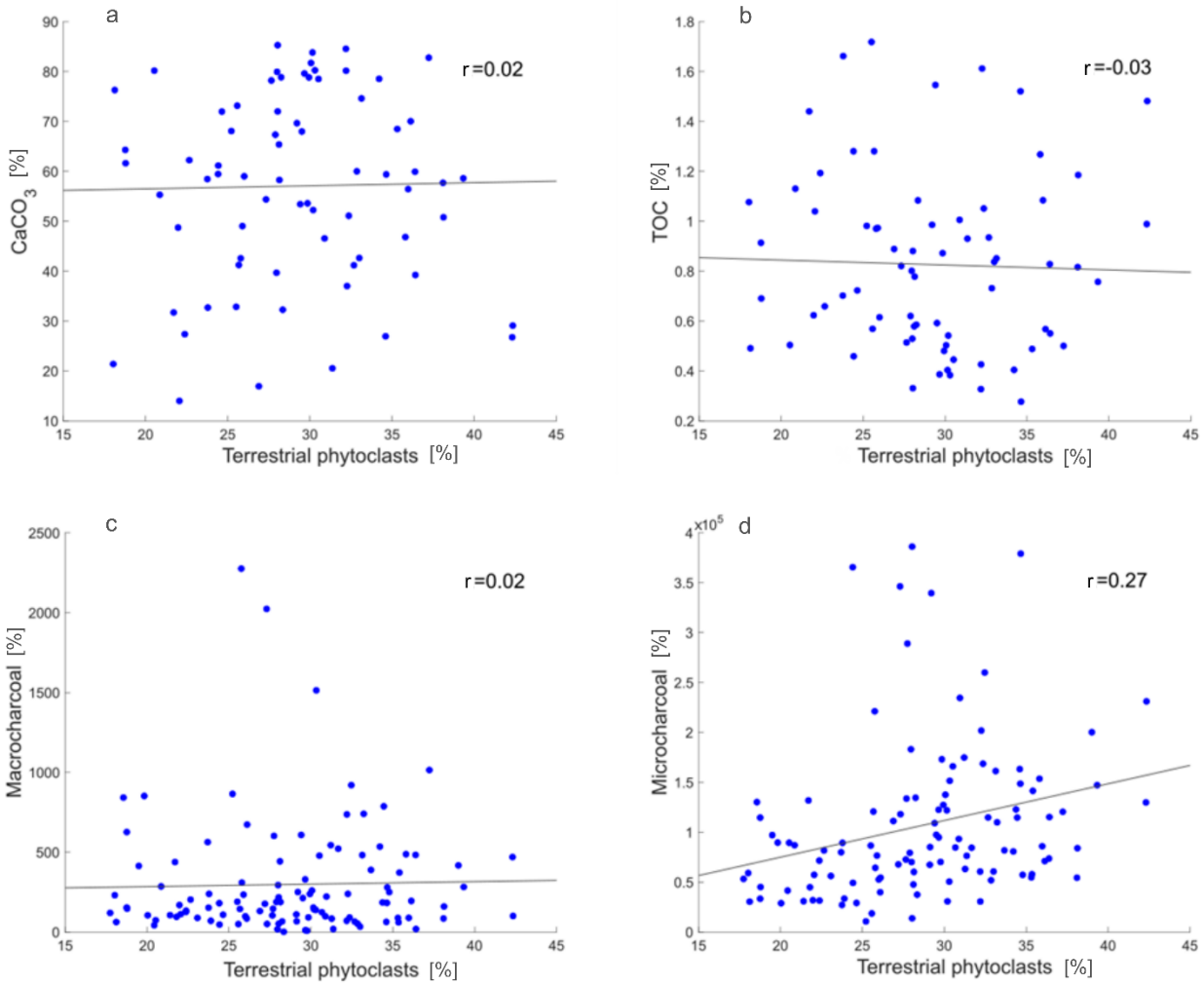

Supplementary Fig. 5: The percentage of terrestrial phytoclasts does not show a correlate with lithological changes (observed in the alternation of TOC-enriched and carbonate-rich sedimentary beds), nor to macrocharcoal abundance. (A) Scatterplot of $CaCO_3$ and the percentage of terrestrial phytoclasts shows no trend. Performing a Pearson correlation provides r=0.02, p=0.8. (B) Scatterplot of TOC and the percentage terrestrial phytoclasts shows no trend. Performing a Pearson's correlation provides r=-0.03, p=0.88. (C) Scatterplot of macrocharcoal and the percentage of terrestrial phytoclasts shows no trend. Performing a Pearson's correlations provides r=0.02, p=0.8. (D) Scatterplot of microcharcoal and the percentage of terrestrial phytoclasts shows a very weak linear trend. Performing a Pearson correlation provides r=0.27; p=0.005, a very weak positive correlation.

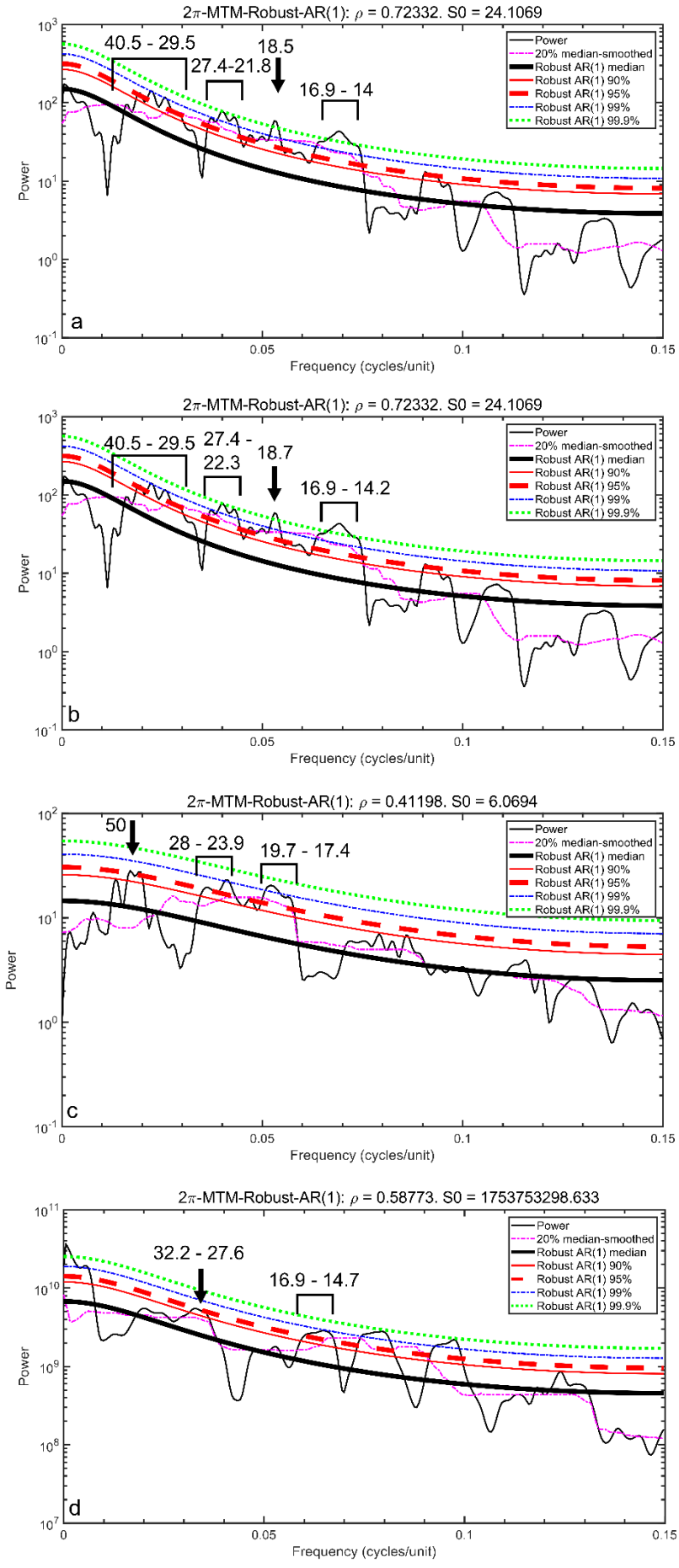

Supplementary Fig. 6: Multi-taper (MTM; 2π) power spectrum of (A) $CaCO_3$, (B) Percentage terrestrial phytoclasts, (C) Illite and (D) Microcharcoal in time domain. This power spectrum was obtained in the Acycle software, with robust red noise models[6]. All records are tuned to the 100 kyr eccentricity of the Ca-XRF record from the Mochras borehole by Ruhl *et al.*[1] spanning the Margaritatus zone, which encompasses the interval studied here. (A) Power spectrum of the $CaCO_3$ record shows strong peaks at the obliquity (~40 kyr) and precession (~26 kyr and ~20 kyr) frequency bands, with a significance level of 99%. (B) Power spectrum of the percentage terrestrial phytoclasts shows one strong power at the precession (~20 kyr) frequency band, with a significance level of 99%. (C) Power spectrum of the relative abundance of illite shows dominant peaks at the obliquity (~40 kyr) and precession frequency (~26 and ~20 kyr) bands at 99% and 99.9% significance respectively. (D) Power spectrum of microcharcoal abundance (normalized to $(Si+Ti+Al+Fe)_{XRF}$ / Ca_{XRF}), showing a periodicity of 32.2–27.6 kyr and 16.9–14.9 kyr at 90 and 95% significance respectively.

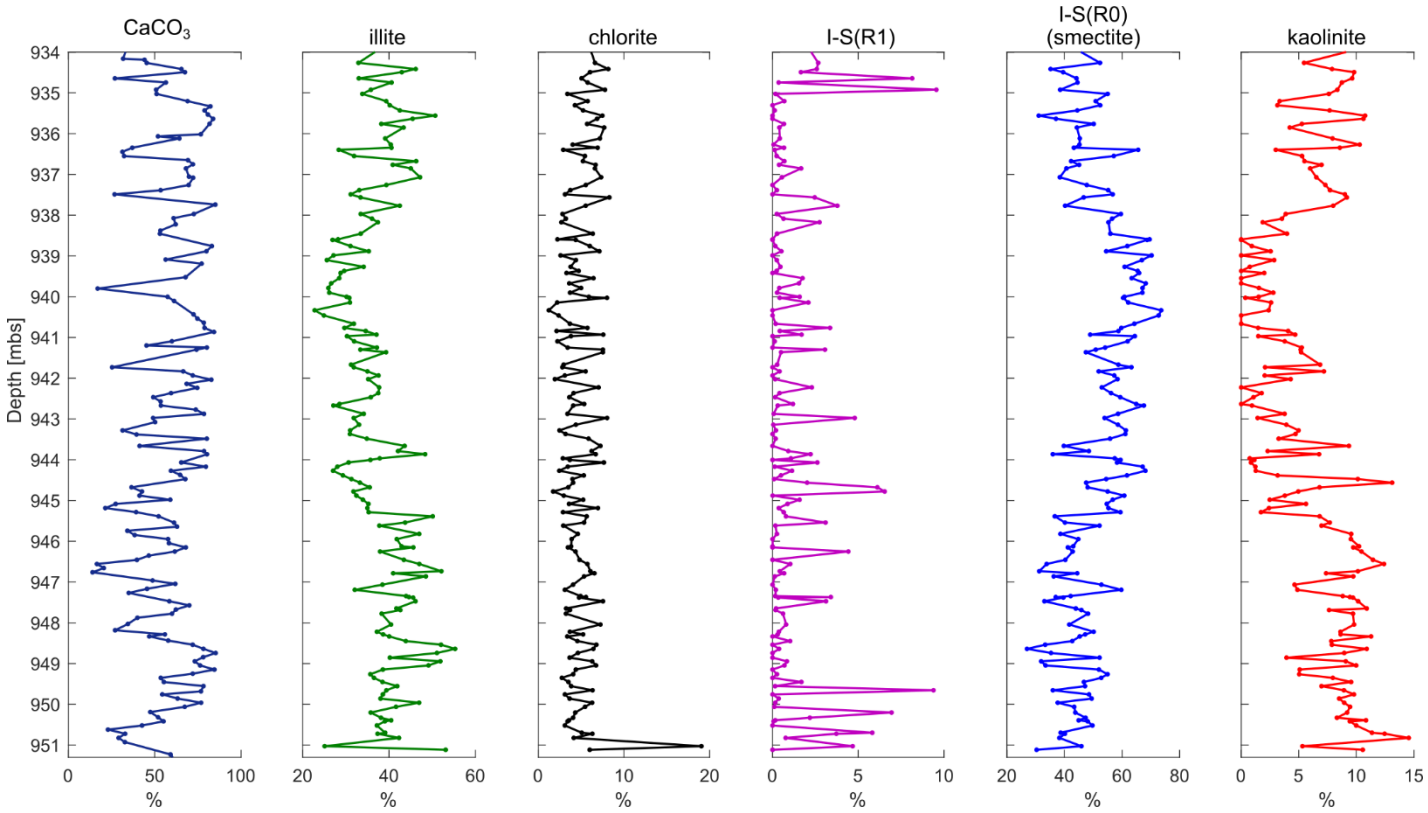

Supplementary Fig. 7: Clay mineralogical abundance from the sediments of the studied interval in the Mochras borehole. The proportions of chlorite and illite-smectite mixed layers type R1 are around the minimum needed for accurate detection (< 5 %) and are therefore not further incorporated in examination of this dataset. A clear long term opposite trend is observed in the abundance of smectite and kaolinite. Kaolinite and illite co-vary over this interval, which is also the case for the longer Pliensbachian clay record of Mochras, indicating a climatic origin in the abundance profile[1]. Metre-scale variations in the percentage of illite corresponds to bedding scale lithological alternations in the studied interval.

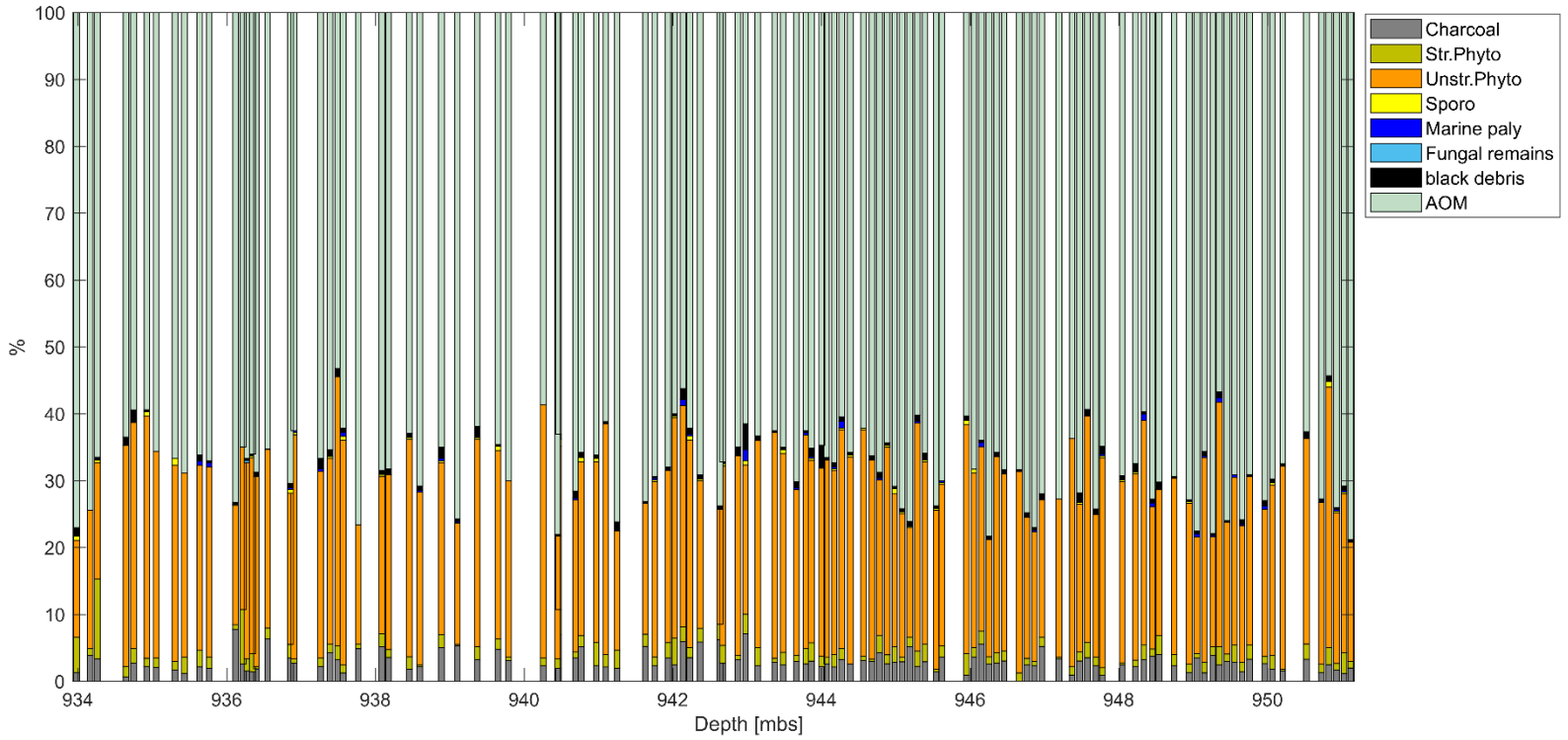

Supplementary Fig. 8: Palynofacies of the studied interval of the Mochras borehole. Relative abundance of the organic particle type identified under the reflective microscope at similar resolution as the charcoal abundance records. In each sample >300 organic particles were identified and grouped based on Oboh-Ikuenobe *et al.*[10]. Amorphous Organic Matter (AOM) is >50 % in all samples and constitutes the main bulk of the marine derived organic matter. The group unstructured phytoclasts is the most abundant organic type with a terrestrial origin. Although minor changes occur in the abundance of phytoclasts and amorphous organic matter, the overall particulate organic composition does not display a large shift.

References

1. Ruhl, M. *et al*. Astronomical constraints on the duration of the Early Jurassic Pliensbachian Stage and global climatic fluctuations. *Earth and Planetary Science Letters*, **455**, 149-165 (2016).
2. Laskar, J., Fienga, A., Gastineau, M. & Manche, H. La2010: a new orbital solution for the long-term motion of the Earth. *Astronomy & Astrophysics*, **532**, A89 (2011).
3. Laskar, J. Astrochronology in *The Geological Time Scale 2020* (eds. Gradstein, F. M., Ogg, J.G., Schmitz, M.D., Ogg, G.M.) 139-158 (Elsevier, 2020).
4. Ogg, J. G., Hinnov, L. A. & Huang, C. Cretaceous in *The geologic time scale* (eds. Gradstein, F. M., Ogg, J.G., Schmitz, M.D., Ogg, G.M.) 793-853 (Elsevier, 2012).
5. Hinnov, L. A. & Hilgen, F. J. Cyclostratigraphy and astrochronology in *The Geologic Time Scale 2012* (eds. Gradstein, F. M., Ogg, J.G., Schmitz, M.D., Ogg, G.M.) 63-83 (Elsevier, 2012).
6. Li, M., Hinnov, L. & Kump, L. Acycle: Time-series analysis software for paleoclimate research and education. *Computers & geosciences*, **127**, 12-22 (2019).
7. Storm, M. S. *et al*. Orbital pacing and secular evolution of the Early Jurassic carbon cycle. *Proceedings of the National Academy of Sciences*, **117**(8), 3974-3982 (2020).
8. Hinnov, L.A., Ruhl, M.R. & Hesselbo, S.P. Reply to the Comment on "Astronomical constraints on the duration of the Early Jurassic Pliensbachian Stage and global climatic fluctuations" (Ruhl *et al*. Earth and Planetary Science Letters, 455 149-165) *Earth and Planetary Science Letters*, **481**, 415-419 (2018).
9. Deconinck, J. F., Hesselbo, S. P. & Pellenard, P. Climatic and sea-level control of Jurassic (Pliensbachian) clay mineral sedimentation in the Cardigan Bay Basin, Llanbedr (Mochras Farm) borehole, Wales. *Sedimentology*, **66**(7), 2769-2783 (2019).
10. Oboh-Ikuenobe, F. E., Obi, C. G., & Jaramillo, C. A. Lithofacies, palynofacies, and sequence stratigraphy of Palaeogene strata in Southeastern Nigeria. *Journal of African Earth Sciences*, **41**(1-2), 79-101, (2005).